The continuity and extension of the domain of validity, the very good accuracy, the rapidity, and the convenience of the use of our charts make it a very precious tool for the engineers.

REFERENCES

[1] A. Ros, R. Daumas, D. Pompei, and E. Rivier, "Variations of the electrical characteristics of an inhomogeneous microstrip line with the dielectric constant of the substrate and with the geometrical dimensions," *IEEE Trans. Microwave Theory Tech.*, vol. MTT-23, pp. 703–708, Aug. 1975.

[2] T. G. Bryant and J. A. Weiss, "Parameters of microstrip transmission lines and coupled pairs of microstrip lines," *IEEE Trans. Microwave Theory Tech.*, vol. MTT-16, pp. 1021–1027, Dec. 1968.

[3] S. V. Judd, I. Whiteley, R. J. Clowes, and D. C. Richard, "An analytical method for calculating miscrostrip transmission line parameters," *IEEE Trans. Microwave Theory Tech.*, vol. MTT-18, pp. 78–87, Feb. 1970.

[4] M. Ramadan and W. F. Westgate, "Impedance of coupled microstrip transmission lines," *Microwave J.*, vol. 14, pp. 30–35, July 1971.

[5] H. A. Wheeler, "Transmission-line properties of parallel strips separated by dielectric sheet," *IEEE Trans. Microwave Theory Tech.*, vol. MTT-13, pp. 173–185, Mar. 1965.

[6] S. Akhtarzad, T. D. Rowbotham, and P. B. Johns, "The design of coupled microstrip lines," *IEEE Trans. Microwave Theory Tech.*, vol. MTT-23, pp. 486–492, June 1975.

[7] L. S. Napoli and J. J. Hughes, "Characteristics of coupled microstrip lines," *RCA Rev.*, vol. 31, pp. 479–498, Sept. 1970.

[8] R. Daumas, D. Pompei, E. Rivier, and A. Ros, "Faster impedance estimation for coupled microstrips with an overrelaxation method," *IEEE Trans. Microwave Theory Tech.*, vol. MTT-21, pp. 552–556, Aug. 1973.

[9] ——, "Some new results on coupled or meanders microstrip line by application of a matricial theory," in *Proc. IEEE Int. Microwave Symp.*, Atlanta, GA, 1974.

Calculation of Microstrip Bends and *Y*-Junctions with Arbitrary Angle

REZA MEHRAN

***Abstract*—A method is described for calculating the frequency-dependent scattering parameters of microstrip bends and *Y*-junctions with arbitrary angles. Use is made of a waveguide model and an orthogonal series expansion for the fields around the discontinuity of the bend, so that the excitation and propagation of higher order modes can be considered. The transmission properties of the *Y*-junctions are derived from those of the bends by a symmetry consideration. Numerical results are given for two different substrates and are compared with experimental data. Neglecting radiation effects, they are in good agreement.**

I. INTRODUCTION

IN THIS PAPER the transmission and reflection properties of microstrip bends of arbitrary angles are investigated theoretically and experimentally. In addition, the results derived for the bends are employed to calculate the scattering matrix of microstrip *Y*-junctions. Design of *Y*-junctions plays a very important role in fabricating microstrip power dividers; if microstrip bends with small declination are connected in series, it should be possible to realize bandpass or bandstop filters. Up to now a calculation method which yields the frequency-dependent scattering parameters of the above mentioned discontinuities has not been described in the literature.

A waveguide mode, which has successfully been employed in earlier papers on other microstrip discontinuities [1]–[5], also is the basis of the theoretical method used in this paper. By employing a similar mathematical procedure, as it is applied in waveguide theory [11], the discontinuity structure is divided into three subareas, which are partly overlapping; for each of the subregions a complete solution of the wave equation is formulated. The continuity conditions governing the electromagnetic fields are satisfied on the surfaces which are common to two adjacent subregions. A system of equations results from this method, from which the unknown field amplitudes, and subsequently the scattering parameters, can be computed. Representative data achieved from the experimental investigations are compared to the theoretical results.

Manuscript received June 8, 1977; revised October 5, 1977.

The author is with the Lehrstuhl für Allgemeine und theoretische Elektrotechnik, Department of Electrical Engineering, University of Duisburg, Duisburg, Germany.

II. FORMULATION OF THE PROBLEM

The waveguide model shown in Fig. 1(b) has been introduced for the microstrip line. It consists of electrical walls at the top and the bottom of the line, and magnetic walls at the sides. The effective width w_{eff} of the model as well as the effective dielectric constant ϵ_{eff} are frequency-dependent model parameters [2], [3]. Making use of this model the properties of the microstrip bend, shown in Fig. 1(c), are calculated. For reasons which will become obvious when calculating the *Y*-junction (Fig. 1(d)), one of the walls may also be chosen to be an electric wall.

The geometrical structure of the bend is subdivided into three regions (Fig. 1(c)), and for each of these subregions

0018-9480/78/0600-0400$00.75

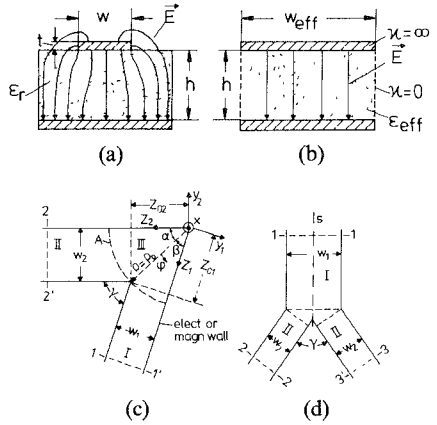

Fig. 1. (a) Cross section of the microstrip line. (b) Waveguide model for the microstrip line. (c) Bend with arbitrary angle. (d) Y-junction with arbitrary angle.

a solution of the wave equation is formulated. Due to the special planar geometry of this discontinuity, only field modes which are transverse magnetic with respect to the x-axis can be excited if the connected microstrip lines transport their fundamental mode (quasi-TEM mode) or TE_{m0}-modes. Therefore in regions I and II the following field equations which describe the superposition of an infinite number of modes propagating in $\pm z$-direction, can be given.

Region I

$$E_x^{\mathrm{I}} = \sum_{m=0}^{\infty} \omega\mu \cdot f_{(m0)}^{\mathrm{I}} \cdot U_{(m0)}^{\mathrm{I}} \cdot \cos\left[\beta_y (y_1 + w_1)\right] \tag{1a}$$

$$H_y^{\mathrm{I}} = \sum_{m=0}^{\infty} f_{(m0)}^{\mathrm{I}} \cdot I_{(m0)}^{\mathrm{I}} \cdot \beta_{z\,(m0)}^{\mathrm{I}} \cdot \cos\left[\beta_y (y_1 + w_1)\right] \tag{1b}$$

$$H_z^{\mathrm{I}} = j \sum_{m=0}^{\infty} \beta_y \cdot f_{(m0)}^{\mathrm{I}} \cdot U_{(m0)}^{\mathrm{I}} \cdot \sin\left[\beta_y (y_1 + w_1)\right] \tag{1c}$$

with

$$f_{(m0)}^{\mathrm{I}} = \sqrt{\frac{\epsilon_{m0}}{w_1 h}} \cdot \frac{\sqrt{y_{(m0)}^{\mathrm{I}}}}{\beta_{z\,(m0)}^{\mathrm{I}}}, \qquad y_{(m0)}^{\mathrm{I}} = \frac{\beta_{z\,(m0)}^{\mathrm{I}}}{\omega\mu}$$

and

$$\left.\begin{matrix} U_{(mo)}^{\mathrm{I}} \\ I_{(m0)}^{\mathrm{I}} \end{matrix}\right\} = a_{1(m0)} \exp\left[-j\beta_z^{\mathrm{I}}(z_1 + z_{01})\right] \pm b_{1(m0)} \exp\left[+j\beta_z^{\mathrm{I}}(z + z_{01})\right] \tag{1d}$$

with

$$\beta_y = \begin{cases} m\pi/w_1, & \text{in the case of magnetic wall} \\ \left(m + \frac{1}{2}\right)\pi/w_1, & \text{in the case of electric wall} \end{cases} \tag{1e}$$

and

$$\epsilon_{\nu 0} = \begin{cases} \left.\begin{matrix} 1 \text{ for } \nu = 0 \\ 2 \text{ for } \nu \neq 0 \end{matrix}\right\}, & \text{in the case of magnetic wall} \\ 2 \text{ for all } \nu, & \text{in the case of electric wall.} \end{cases} \tag{1f}$$

Region II

$$E_x^{\mathrm{II}} = \sum_{p=0}^{\infty} \omega\mu \cdot f_{(p0)}^{\mathrm{II}} \cdot U_{(p0)}^{\mathrm{II}} \cdot \cos\left[\frac{p\pi}{w_2}(y_2 + w_2)\right] \tag{2a}$$

$$H_y^{\mathrm{II}} = -\sum_{p=0}^{\infty} \beta_{z\,(p0)}^{\mathrm{II}} \cdot f_{(p0)}^{\mathrm{II}} \cdot I_{(p0)}^{\mathrm{II}} \cdot \cos\left[\frac{p\pi}{w_2}(y_2 + w_2)\right] \tag{2b}$$

$$H_z^{\mathrm{II}} = j \sum_{p=0}^{\infty} (p\pi/w_2) \cdot f_{(p0)}^{\mathrm{II}} \cdot U_{(p0)}^{\mathrm{II}} \cdot \sin\left[\frac{p\pi}{w_2}(y_2 + w_2)\right] \tag{2c}$$

with

$$f_{(p0)}^{\mathrm{II}} = \sqrt{\frac{\epsilon_{p0}}{w_2 h}} \cdot \frac{\sqrt{y_{(p0)}^{\mathrm{II}}}}{\beta_{z\,(p0)}^{\mathrm{II}}} \tag{2d}$$

and

$$\left.\begin{matrix} U_{(p0)}^{\mathrm{II}} \\ I_{(p0)}^{\mathrm{II}} \end{matrix}\right\} = a_{2(p0)} \exp\left[j\beta_z^{\mathrm{II}}(z_2 - z_{02})\right] \pm b_{2(p0)} \exp\left[-j\beta_z^{\mathrm{II}}(z_2 - z_{02})\right] \tag{2e}$$

and

$$\epsilon_{p0} = \begin{cases} 1 \text{ for } p = 0 \\ 2 \text{ for } p \neq 0. \end{cases} \tag{2f}$$

In subregion III the following field components E_x^{III} and H_φ^{III} can be formulated in a cylindrical coordinate system:

$$E_x^{\mathrm{III}} = -\sum_{q=0}^{\infty} j\omega\mu \cdot c_{(q0)} \sqrt{\frac{\epsilon_{q0}}{\gamma h}} \cdot j_\nu\left(\beta_{(q0)}^{\mathrm{III}} \cdot \zeta\right) \cdot \cos\left[\beta_\varphi(\varphi + \alpha)\right] \tag{3a}$$

$$H_\varphi^{\mathrm{III}} = -\sum_{q=0}^{\infty} c_{(q0)} \sqrt{\frac{\epsilon_{q0}}{\gamma h}} \cdot \tilde{j}_\nu\left(\beta_{(q0)}^{\mathrm{III}} \cdot \zeta\right) \cos\left[\beta_\varphi(\varphi + \alpha)\right] \tag{3b}$$

with

$$\beta_{(q0)}^{\mathrm{III}} = \omega\sqrt{\epsilon^{\mathrm{III}}\mu} \qquad \nu = q\pi/\gamma \tag{3c}$$

and

$$\beta_\varphi = \begin{cases} q\pi/\gamma, & \text{in the case of magnetic wall} \\ \left(q + \frac{1}{2}\right)\pi/\gamma, & \text{in the case of electric wall.} \end{cases} \tag{3d}$$

In (1d) and (2e) the quantities $a_{1(m0)}$, $a_{2(p0)}$, $b_{1(m0)}$, and $b_{2(p0)}$ denote the normalized field amplitudes of the incident and reflected waves, respectively, whereas $c_{(q0)}$ in (3a) and (3b) are the normalized amplitudes of the standing waves in region III. $j_\nu(\beta_{(q0)}^{\mathrm{III}} \cdot \zeta)$ and $\tilde{j}_\nu(\beta_{(q0)}^{\mathrm{III}} \cdot \zeta)$ are the Bessel functions of order $q\pi/\gamma$ and argument $\beta_{(q0)}^{\mathrm{III}} \cdot \zeta$ and their first derivatives due to ζ, respectively.

III. Mathematical Solution of the Problem

The continuity conditions require the matching of the tangential electromagnetic subregional fields at the suit-

able common interface A (Fig. 1(c)). With the continuity condition for the electric field components at $\zeta=\zeta_0$:

$$E_x^{\mathrm{III}}=\begin{cases}E_x^{\mathrm{II}}, & \text{for } -\alpha\leqq\varphi\leqq 0\\ E_x^{\mathrm{I}}, & \text{for } 0\leqq\varphi\leqq\beta\end{cases} \tag{4}$$

and by multiplying the fields with the eigenfunctions associated with region III and integrating over the interval $-\alpha\leqq\varphi\leqq\beta$ the following series expansion can be derived for the normalized field amplitudes $c_{(Q0)}$ in subregion III:

$$\begin{aligned}c_{(Q0)}\cdot J_Q\left(\beta^{\mathrm{III}}_{(Q0)}\cdot\zeta_0\right)=&\sum_{p=0}^{\infty} j\sqrt{\frac{\epsilon_{p0}}{w_2\gamma}}\cdot\frac{\sqrt{y^{\mathrm{II}}_{(p0)}}}{\beta^{\mathrm{II}}_{z\,(p0)}}\\ &\cdot\left[a_{2(p0)}\cdot F_2^{+}{}_{(pQ)}+b_{2(p0)}\cdot F_2^{-}{}_{(pQ)}\right]\\ &+\sum_{m=0}^{\infty} j\sqrt{\frac{\epsilon_{m0}}{w_1\cdot\gamma}}\cdot\frac{\sqrt{y^{\mathrm{I}}_{(m0)}}}{\beta^{\mathrm{I}}_{z\,(m0)}}\\ &\cdot\left[a_{1(m0)}\cdot F_1^{+}{}_{(mQ)}+b_{1(m0)}\cdot F_1^{-}{}_{(mQ)}\right]\end{aligned} \tag{5a}$$

with

$$\begin{aligned}F_1^{\pm}{}_{(Qm)}=&\sqrt{\epsilon_{Q0}}\cdot\int_0^{\beta}\cos\left[\beta_y^{\mathrm{I}}(w_1-\zeta_0\sin(\beta-\varphi))\right]\\ &\cdot\cos\left[\beta_\varphi(\varphi+\alpha)\right]\\ &\cdot\exp\left[\pm j\beta^{\mathrm{I}}_{z\,(m0)}(\zeta_0\cos(\beta-\varphi)-z_{01})\right]\end{aligned} \tag{5b}$$

and

$$\begin{aligned}F_2^{\pm}{}_{(Qp)}=&\sqrt{\epsilon_{Q0}}\int_{-\alpha}^{0}\cos\left[\frac{p\pi}{w_2}(w_2-\zeta_0\sin(\alpha+\varphi))\right]\\ &\cdot\cos\left[\beta_\varphi(\varphi+\alpha)\right]\\ &\cdot\exp\left[\pm j\beta^{\mathrm{II}}_{z\,(p0)}(\zeta_0\cos(\alpha+\varphi)-z_{02})\right].\end{aligned} \tag{5c}$$

If the continuity condition for the magnetic field components at $\zeta=\zeta_0$:

$$H_\varphi^{\mathrm{III}}=\begin{cases}-H_z^{\mathrm{II}}\sin(\varphi+\alpha)-H_y^{\mathrm{II}}\cos(\varphi+\alpha), & \text{for } -\alpha<\varphi<0\\ -H_z^{\mathrm{I}}\sin(\beta-\varphi)+H_y^{\mathrm{I}}\cos(\beta-\varphi), & \text{for } 0<\varphi<\beta\end{cases} \tag{6}$$

is applied, a corresponding expression can be derived by field expansion in regions I and II with respect to the eigenfunctions of region III:

$$\begin{aligned}c_{(Q0)}\cdot\tilde{J}_\nu\left(\beta^{\mathrm{III}}_{(Q0)}\zeta_0\right)=&\sum_{p=0}^{\infty} j\sqrt{\frac{\epsilon_{p0}}{w_2\gamma}}\cdot\frac{\sqrt{y^{\mathrm{II}}_{(p0)}}}{\beta^{\mathrm{II}}_{z\,(p0)}}\\ &\cdot\left[a_{2(p0)}\frac{\partial F_2^{+}{}_{(pQ)}}{\partial\zeta}+b_{2(p0)}\cdot\frac{\partial F_2^{-}{}_{(pQ)}}{\partial\zeta}\right]\\ &+\sum_{m=0}^{\infty} j\sqrt{\frac{\epsilon_{m0}}{w_1\gamma}}\cdot\frac{\sqrt{y^{\mathrm{I}}_{(m0)}}}{\beta^{\mathrm{II}}_{z\,(m0)}}\\ &\cdot\left[a_{1(m0)}\frac{\partial F_1^{+}{}_{(mQ)}}{\partial\zeta}+b_{1(m0)}\frac{\partial F_1^{-}{}_{(mQ)}}{\partial\zeta}\right].\end{aligned} \tag{7}$$

By eliminating the unknown normalized field amplitudes $c_{(Q0)}$ from (5) and (7), an infinite system of equations results. Since the amplitudes of the incident waves are known the system is deterministic, and after truncation of the sums the field amplitudes of the reflected waves in regions I and II can be computed.

IV. Scattering Parameters of the Bend and of the Y-Junction

With the functional dependence of the amplitudes of the reflected waves in both regions on those of the incident waves in one region available, the scattering parameters easily can be calculated by the definition $s_{ik}=b_i/a_k$, where (b_i) is the normalized field amplitude of the reflected wave and (a_k) that of the incident wave. If excitation at port 1 (Fig. 1(c)) prevails, the following system of equations is valid for the scattering parameters s_{11}^B and s_{21}^B of the bend:

$$\begin{aligned}&\sum_{p=0}^{\infty}\left[G_{1\,(Qp)}^{\mathrm{II}}\cdot F_2^{-}{}_{(Qp)}-G_{2\,(Qp)}^{\mathrm{II}}\frac{\partial F_2^{-}{}_{(Qp)}}{\partial\zeta}\right]s^B_{21(p0)}\\ &\quad+\sum_{m=0}^{\infty}\left[G_{1(Qm)}^{\mathrm{I}}\cdot F_1^{-}{}_{(Qp)}-G_{2(Qm)}^{\mathrm{I}}\frac{\partial F_1^{-}{}_{(Qm)}}{\partial\zeta}\right]s^B_{11(m0)}\\ &=G_{2(QM)}^{\mathrm{I}}\frac{\partial F_1^{+}{}_{(QM)}}{\partial\zeta}-G_{1(QM)}^{\mathrm{I}}\cdot F_1^{+}{}_{(QM)}\end{aligned} \tag{8a}$$

with

$$\begin{aligned}G_{1,2(Qp)}^{\mathrm{II}}=&j\sqrt{\frac{\epsilon_{p0}}{w_2\gamma}}\cdot\frac{\sqrt{y^{\mathrm{II}}_{(p0)}}}{\beta^{\mathrm{II}}_{z\,(p0)}}\\ &\cdot\begin{cases}\dfrac{1}{J_\nu\left(\beta^{\mathrm{III}}_{(Q0)}\cdot\zeta_0\right)}, & \text{for } G_1^{\mathrm{II}}\\ \dfrac{1}{\tilde{J}_\nu\left(\beta^{\mathrm{III}}_{(Q0)}\cdot\zeta_0\right)}, & \text{for } G_2^{\mathrm{II}}\end{cases}\end{aligned} \tag{8b}$$

$$\begin{aligned}G_{1,2(Qm)}^{\mathrm{I}}=&j\sqrt{\frac{\epsilon_{m0}}{w_1\gamma}}\cdot\frac{\sqrt{y^{\mathrm{I}}_{(m0)}}}{\beta^{\mathrm{I}}_{z\,(m0)}}\\ &\cdot\begin{cases}\dfrac{1}{J_\nu\left(\beta^{\mathrm{III}}_{(Q0)}\cdot\zeta_0\right)}, & \text{for } G_1^{\mathrm{I}}\\ \dfrac{1}{\tilde{J}_\nu\left(\beta^{\mathrm{III}}_{(Q0)}\cdot\zeta_0\right)}, & \text{for } G_2^{\mathrm{II}}\end{cases}\end{aligned} \tag{8c}$$

In order to calculate the scattering parameters s_{22}^B and s_{12}^B, the bend must be excited at port 2 (Fig. 1(c)). Consequently the scattering parameters $s^B_{21(p0)}$ and $s_{11(m0)}$ on the left-hand side, and the expressions $F^+_{1(QM)}$ and their first derivatives as well as $G^{\mathrm{I}}_{1,2}$ on the right-hand side of (8a), must be replaced by $s^B_{22(p0)}$ and $s^B_{12(m0)}$ or $F^+_{2(QP)}$ and their first derivatives as well as $G^{\mathrm{II}}_{1,2}$, respectively.

In order to decide how many modes have to be considered in the expansion of the fields, the convergence be-

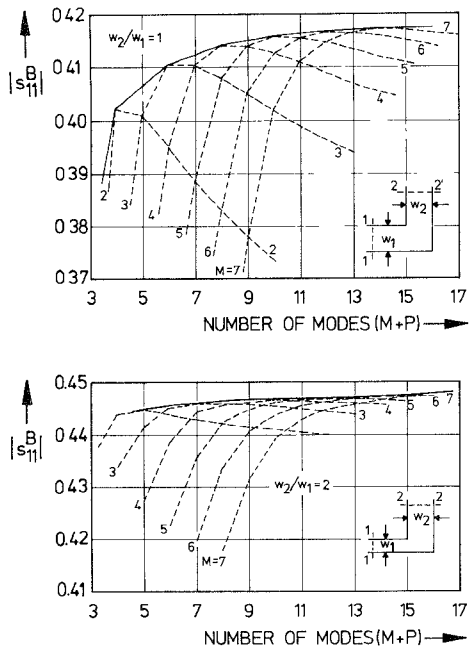

Fig. 2. The dependence of the transmission coefficient $|s_{11}^B|$ of the bend on the sum of mode numbers in the regions I and II $M+P$ ($\epsilon_r=2.32$, $w_1=0.438$ cm, $h=0.156$ cm, $f=7$ GHz).

havior of the method has been investigated. In Fig. 2 the absolute value of the reflection coefficients $|s_{11}^B|$ of a 90° bend are shown as a function of the considered higher order modes in regions I and II. The number of the higher order modes to be considered in region III always is equal to the sum of the higher order modes in regions I and II. It is clearly demonstrated that the method exhibits the relative convergence phenomenon, e.g., [6], [7]. Therefore, convergence to the correct physical values only is given, if the mode numbers (M and P) in regions I and II are related to the effective widths (w_1 and w_2) of the lines by $M/P \approx w_1/w_2$.

The scattering parameters of the Y-junction can be deduced from that of the bend. This is done by alternative even- and odd-mode excitation at opposite ports and application of the superposition principle. If the Y-junction is excited symmetrically (the incident waves are of equal phase and amplitude) at ports 2 and 3, the symmetry plane S in region I (Fig. 1(d)) can be replaced by a magnetic wall. An electric wall in the symmetry plane is assumed in the case of an antisymmetric excitation (the incident waves have the same amplitude but a phase-difference of 180°). This procedure leads to the following relationship between the scattering parameters of the Y-junction s_{ij}^Y and that of the bend s_{ij}^B:

$$s_{21}^Y = s_{12m}^B/\sqrt{2}\,, \quad s_{11}^Y = s_{11m}^B$$
$$s_{22}^Y = \frac{(s_{22m}^B + s_{22e}^B)}{2}\,, \quad s_{23}^Y = \frac{(s_{22m}^B - s_{22e}^B)}{2}\,. \tag{9}$$

The subscripts e and m indicate that the elements s_{ij}^B are those of the bend with an electric or a magnetic wall, respectively (Fig. 1(c)).

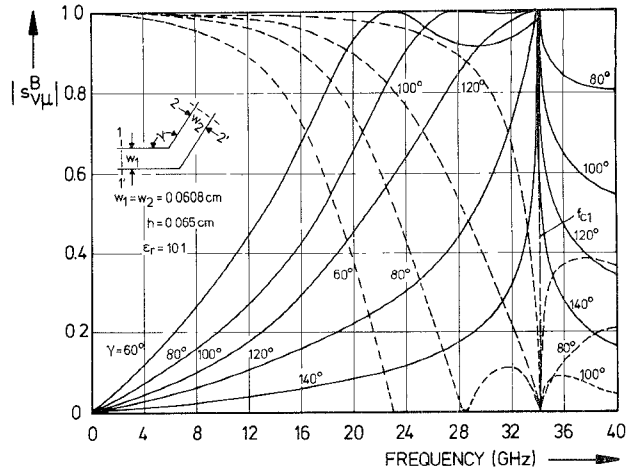

Fig. 3. Numerical results for the reflection and transmission coefficient of the bend with different angle γ in dependence on the frequency f ($—|s_{11}^B|$, $—|s_{21}^B|$).

V. Results

The scattering parameters of microstrip bends with arbitrary angle between the lines have been computed from the truncated system of equations (8a). The method is not restricted to lines of equal widths. However, the angle between the lines ($\gamma > 90°$) and the effective widths (w_1, w_2) must obey the relation

$$\cos(180° - \gamma) \leqq w_1/w_2, \qquad \text{for } w_1 < w_2. \tag{10}$$

Only in this case the matching of the fields in the three regions can be achived on a common interface.

As will be shown in Section VI the characteristic of the s-parameters for the bends with small angle γ, calculated from the model bend (Fig. 1c), are shifted to smaller frequencies if compared to the measured results. The displacement increases with decreasing angle γ. These discrepancies between theory and measurement are due to the fact that for bends with small angle γ, which have a stronger coupling from one line to another near the bend, the fringing field at the corner of the bend is overestimated by the radius ζ_0 in the region III (model bend). In order to achive good coincidence between theory and measurements, an effective radius ζ_{eff} in region III is taken into account. This radius ζ_{eff} and the dielectric constant $\epsilon_{\text{eff}}^{\text{III}}$ are calculated from physical values by considering the fringing field as it was done by Wheeler [8], [9]. In the computation of the results plotted for the bends with small angle γ in this paper, the radius ζ_{eff}, and consequently a new angle relation, are considered. The introduction of the radius ζ_{eff} should only be understood as a correction of the computed results, since by the consideration of ζ_{eff}, the exact matching of the fields at a common interface may be slightly injured.

Fig. 3 shows how for different angles the modules of the TEM-scattering parameters s_{11}^B and s_{21}^B of bends with equal widths ($w_1 = w_2$) depend on the frequency f. The reflection coefficient $|s_{11}^B|$ increases with f in the frequency-range $0 < f < f_{c1}$, where f_{c1} is the cutoff-frequency of the first higher order (TE_{10}) mode [2], [3].

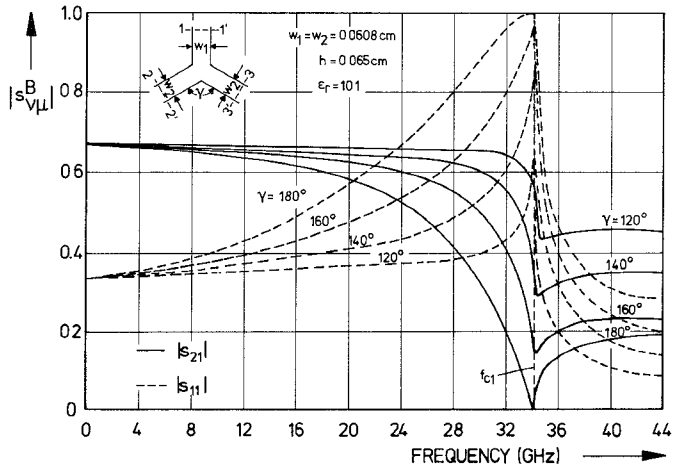

Fig. 4. Numerical results for the reflection and transmission coefficient of the Y-junction with equal field impedance ($z_{w1} = z_{w2}$) and different angle γ in dependence on the frequency f.

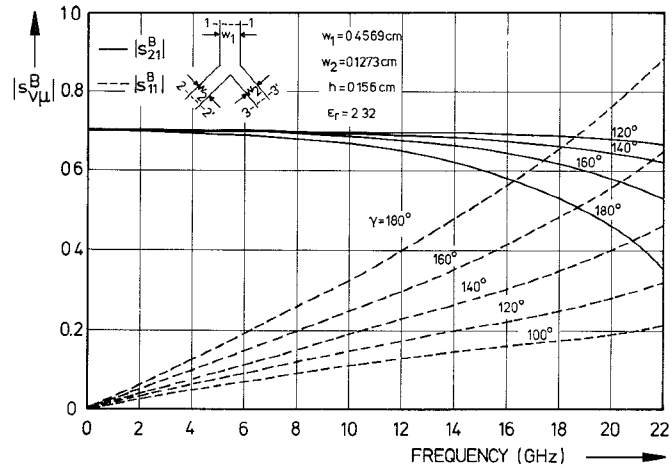

Fig. 5. Numerical results for the reflection and transmission coefficient of the Y-junction with different field impedance ($z_{w1} = z_{w2}/2$) and angle γ in dependence on the frequency f.

Correspondingly, the transmission coefficient $|s^B_{21}|$ decreases with f. For frequencies $f > f_{c1}$, a part of the power is transmitted into the TE_{10}-mode, so that the transmission coefficient $|s^B_{21}|$ of the TEM-mode is always smaller than that for $f = 0$. If the angle γ is small, there exists a frequency f_0 in the frequency range $f < f_{c1}$ at which the transmission or reflection coefficient (s^B_{21} or s^B_{11}) vanishes. With this the bend attains a bandpass or bandstop character.

The scattering parameters of the symmetric Y-junction can be calculated from (8a) and (9). Computed results are presented in Figs. 4 and 5. The modulus of the reflection coefficients $|s^Y_{11}|$ and transmission coefficients $|s^Y_{21}|$ are plotted in dependence on the frequency f. The field impedance of the microstrip lines I and II are either equal ($z_{w1} = z_{w2}$) or different ($z_{w1} = z_{w2}/2$). The argumentation given for the reflected and transmitted power of the bend is valid for the Y-junction, too.

VI. Conclusion

A method has been proposed for the computation of the scattering parameters of microstrip bends and Y-junctions having an arbitrary angle between the lines. Measurements have been performed to verify its validity.

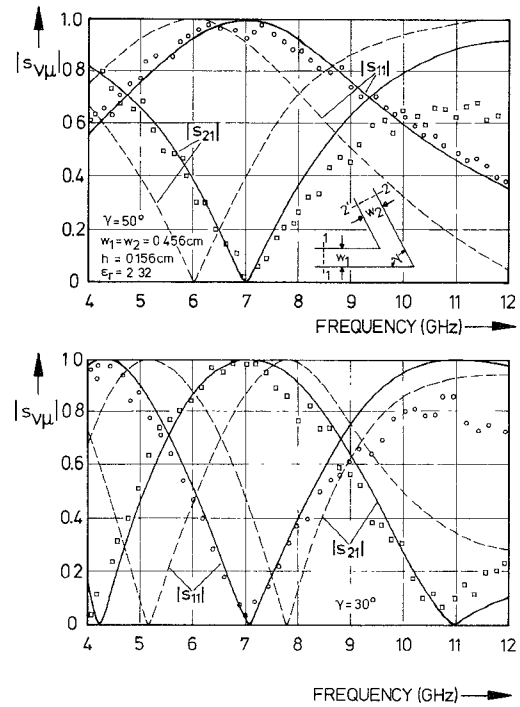

Fig. 6. Comparison between the theoretical and experimental results for the reflection and transmission coefficient $|s^B_{11}|$ and $|s^B_{21}|$ of the bend.

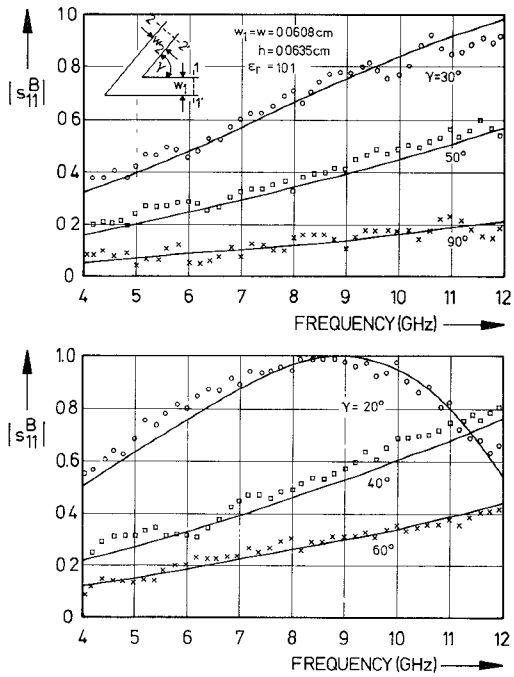

Fig. 7. Comparison between the theoretical and experimental results for the reflection coefficient $|s^B_{11}|$ of the bend.

Figs. 6–8 show a few examples of theoretical and experimental results. The measurements are carried out with a HP-network analyser using the sliding-load method [10]. The influence of the coaxial-to-microstrip transitions and line-losses is eliminated by a computer-aided calibration procedure. However it is difficult to reproduce the transitions by calibration and measurement exactly. Therefore, the mismatching of the coaxial to microstrip line cannot be considered by the correction procedure completely. So, a fluctuation of measurement results can be established. The dotted curves in Fig. 6 have been computed utilizing

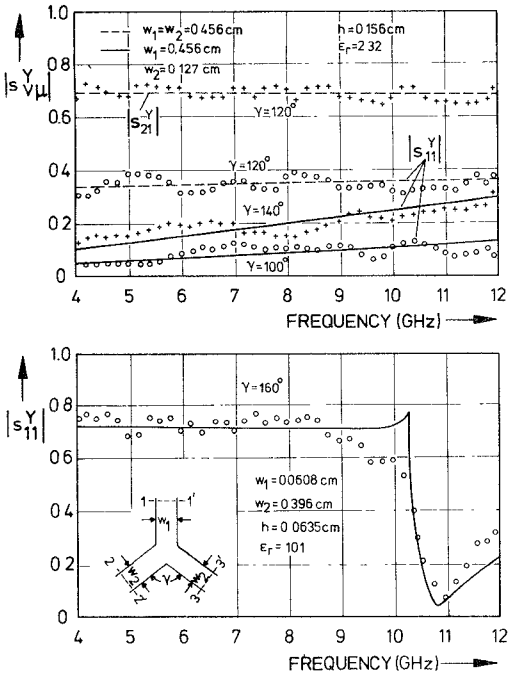

Fig. 8. Comparison between the theoretical and experimental results for the reflection and transmission coefficient and $|s^Y_{11}|$ of the Y-junction.

the model-bend with the radius ζ_0 of the region III, as it is mentioned in Section V. They are shifted to lower frequencies. For the bends, a good agreement between theory and experiment is found, if the effective radius ζ_{eff} is taken into account in region III. Discrepancies between measurement and results obtained from the theory especially occur if the dielectric constant ϵ_r of the substrate material is small and the frequency is high. This is due to radiation effects which then are of pronounced influence for frequencies near the higher order mode cutoff-frequencies (Figs. 6 and 8(b)).

Nomenclature

- $a_{(\nu 0)}$ Normalized field amplitudes of the incident waves.
- $b_{(\nu 0)}$ Normalized field amplitudes of the reflected waves.
- $c_{(\nu 0)}$ Normalized field amplitudes of the standing waves.
- E_x x-component of the electric field.
- H_y y-component of the magnetic field.
- H_z z-component of the magnetic field.
- H_φ φ-component of the magnetic field.
- $J_\nu(x)$ Bessel function of order ν and argument x.
- $J'_\nu(x)$ First derivative of the Bessel function with respect to ζ-axis.
- $s_{\nu\mu}$ Scattering parameters.
- m,p,q Mode number.
- ω Angular frequency.
- ϵ Permittivity equals $\epsilon_0 \cdot \epsilon_{\text{reff}}$; ϵ_{reff} is the relative effective permittivity.
- μ Permeability equals $\mu_0 \cdot \mu_r$.
- k Dominant wave number equals $\omega\sqrt{\epsilon\mu}$.
- $\beta_{z(\nu 0)}$ Guide wave number equals $\sqrt{k^2-\beta^2_{x(\nu 0)}}$.
- $y_{(\nu 0)}$ Guide characteristic admittance equals $\beta_{z(\nu 0)}/\omega\mu$.

References

[1] I. Wolff, G. Kompa, and R. Mehran, "Calculation method for microstrip discontinuities and T-junctions," *Electron. Lett.*, vol. 8, pp. 177–179, Apr.1972.

[2] G. Kompa and R. Mehran, "Planar waveguide model for calculating microstrip components," *Electron. Lett.*, vol. 11, pp. 459–460, Sept. 1975.

[3] R. Mehran, "The frequency-dependent scattering matrix of microstrip right-angle bends, T-junctions and crossings," *Arch. Elek. Ubertrangung*, vol. 29, pp. 454–460, Nov. 1975.

[4] G. Kompa, "S-matrix computation of microstrip discontinuities with a planar waveguide model," *Arch. Elek. Ubertragung*, vol. 30, pp. 58–64, Feb. 1976.

[5] W. Menzel and I. Wolff, "A method for calculating the frequency dependent properties of microstrip discontinuities," *IEEE Trans. Microwave Theory Tech.*, vol. MTT-25, pp. 107–112, Feb. 1977.

[6] S. Wu Lee and W. R. Jones, "Convergence of numerical solution of iristype discontinuity problem," *IEEE Trans. Microwave Theory Tech.*, vol. MTT-19, pp. 528–536, 1971.

[7] R. Mittra and T. Itoh, "Analytical and numerical studies of the relative convergence phenomenon arising in the solution of an integral equation by the moment method," *IEEE Trans. Microwave Theory Tech.*, vol. MTT-20, pp. 96–104, Feb. 1972.

[8] H. A. Wheeler, "Transmission-line properties of parallel wide strips by a conformal mapping approximation," *IEEE Trans. Microwave Theory Tech.*, vol. MTT-12, 1964.

[9] H. A. Wheeler, "Transmission-line properties of parallel strips separated by a dielectric sheet," *IEEE Trans. Microwave Theory Tech.*, vol. MTT-13, pp. 172–185, 1965.

[10] G. Kompa, "Dispersion measurements of the first two higher-order modes in open microstrip," *Arch. Elek. Ubertragung*, vol. 19, pp. 182–185, 1975.

[11] F. Reisdorf, "Analysis and design of broadband-matched multistage angle bends in rectangular waveguides," *Frequenz*, vol. 30, pp. 126–131, 1976.